THE JOURNAL OF PHYSICAL CHEMISTRY C

ARTICLE

pubs.acs.org/JPCC

Enhanced Lithium-Ion Intercalation Properties of V_2O_5 Xerogel Electrodes with Surface Defects

Dawei Liu,[†] Yanyi Liu,[†] Anqiang Pan,[†,‡] Kenneth P. Nagle,[§] Gerald T. Seidler,[§] Yoon-Ha Jeong,[⊥] and Guozhong Cao*[,†]

[†]Department of Materials Science and Engineering, University of Washington, Seattle, Washington, United States

[‡]Department of Materials Science and Engineering, Central South University, Changsha, China

[§]Department of Physics, University of Washington, Seattle, Washington, United States

[⊥]National Center for Nanomaterials Technology (NCNT), Pohang University of Science and Technology, Pohang, South Korea

ABSTRACT: V_2O_5 xerogel films were fabricated by casting V_2O_5 sols onto fluorine-doped tin oxide (FTO) glass substrates and annealing at 300 °C for 3 h in different annealing atmospheres of air and nitrogen. Films prepared in different annealing conditions possess different grain sizes and crystallinity, while the vanadium ion oxidation state also varies, as identified by X-ray absorption spectroscopy. A nitrogen annealing atmosphere induces the presence of defects, such as V^{4+} ions, and associated oxygen vacancies. Thus, the presence of defects, whether on the film surface or in the bulk, can be controlled by using air and nitrogen annealing atmospheres in the proper order. Electrochemical impedance analyses reveal enhanced charge-transfer conductivity in films with more V^{4+} and oxygen vacancies on the film surface, that is, a film annealed, first, for 0.5 h in air and then for 2.5 h in nitrogen. Lithium-ion intercalation measurements show that, at a charge/discharge current density of 600 mA g^{-1}, this film possesses a noticeably better lithium-ion storage capability than films without surface defects. This sample starts with an initial discharge capacity of 139 mA h g^{-1}, and the capacity increases slowly to a maximum value of 156 mA h g^{-1} in the 15th cycle, followed by a mild capacity degradation in later cycles. After 50 cycles, the discharge capacity is still as high as 136 mA h g^{-1}. A much improved lithium-ion intercalation capacity and cyclic stability are attributed to V^{4+} surface defects and associated oxygen vacancies introduced by N_2 annealing.

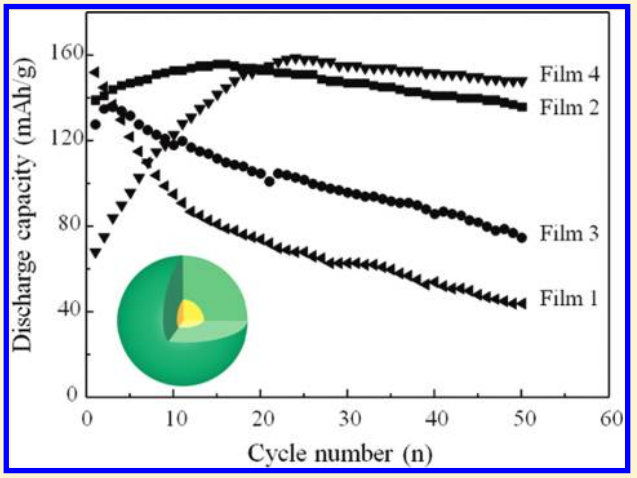

1. INTRODUCTION

Vanadium pentoxide (V_2O_5) has been intensively studied for the past decades since the first report of its lithium-ion intercalation capability by Whittingham et al.[1] It is a favorable candidate as a lithium-ion intercalation electrode because of its layered structure, which is open to reversible lithium-ion insertion/extraction and nontoxic chemical properties, which enable "green" energy storage.[2−5] Xerogel film, which has good chemical stability and whose porous structure provides a high surface area, is one of the most favorable structures of vanadium pentoxide for lithium-ion intercalation.[6,7] Many studies have been focused on making xerogel films with high intercalation capability and cyclic stability by controlling physical and chemical characteristics.[9−11] Crystallinity is found to be one of the factors that affects the intercalation performance of xerogel films.[12−14] Because of the less well packed structure, which can accommodate more lithium ions, vanadium pentoxide xerogel film with a more hydrous structure could have a higher intercalation capacity and better cyclic stability than well-crystallized orthorhombic film. Recently, we found that the presence of defects, such as V^{4+} ions, and associated oxygen vacancies on the film surface could also contribute to the improvement of the cyclic stability of repeated lithium-ion intercalation/deintercalation processes.[15] The presence of defects at the electrode/electrolyte interface could possibly facilitate the phase transition experienced during lithium reactions due to modified surface thermodynamics.[16,17] In addition, the presence of surface defects at the electrode/electrolyte interface could well preserve the integrity of the electrode surface morphology, improving the cyclic stability of intercalation electrodes.[18] Surface defects on vanadium oxide xerogel films can be introduced by annealing hydrous films in an inert gas environment at elevated temperatures, such as nitrogen gas at 300 °C.[19,20] In addition to introducing surface defects, nitrogen annealing also induces a less crystallized structure, for

Received: December 13, 2010
Revised: February 12, 2011
Published: March 03, 2011

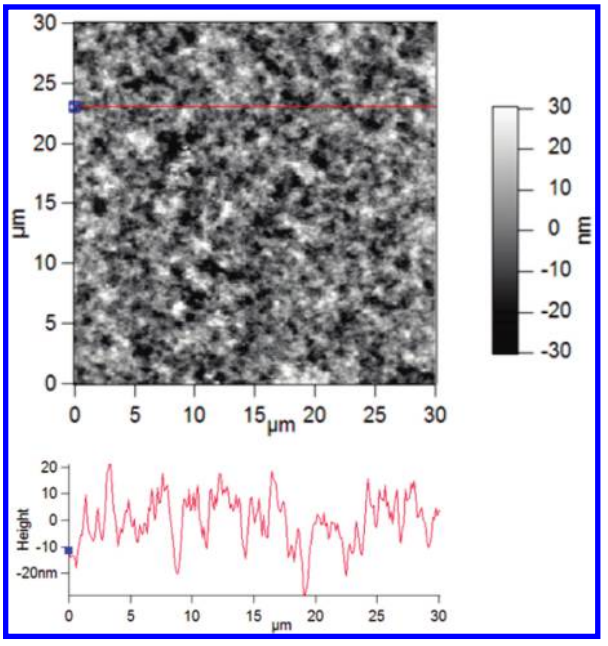

Figure 1. Topographical AFM image (30 μm × 30 μm) of the V_2O_5 xerogel film surface after thermal treatment, showing the roughness of about 50 nm on the red line.

example, a larger interlayer distance and smaller grain size, as compared with annealing in air under identical conditions.[15] Films annealed in nitrogen gas at 300 °C for 3 h are identified with both low crystallinity and discernible surface defects and found to possess obviously improved cyclic stability when compared with films with high crystallinity and few surface defects. However, the contributions from the degree of crystallinity and the density of surface defects could not be isolated due to their coexistence in these films. To identify the contribution of surface defects to lithium-ion intercalation properties, the advantages of low crystallinity have to be eliminated. This can be accomplished by using combined air and nitrogen gas annealing in a proper manner. In our experiments, we annealed sol−gel-derived V_2O_5 xerogel films in air and nitrogen with alternating orders. The fabricated xerogel films can have good crystallinity with surface defects or poor crystallinity with no surface defects. The relationships between annealing atmospheres and induced crystallinity, the presence of defects in the V_2O_5 film, and lithium-ion intercalation properties are discussed.

2. EXPERIMENTAL SECTION

A diluted sol of $V_2O_5 \cdot nH_2O$ was prepared using the method reported by Fontenot et al.[21] In brief, 0.136 g of V_2O_5 powder was dissolved in 2 mL of deionized water and 0.603 mL of 30% H_2O_2 solution. The suspension was stirred until the V_2O_5 powder totally dissolved, resulting in a clear and dark red solution. The solution was then sonicated to get a yellow-brown gel that was dispersed into deionized water in a molar concentration of 0.005 M with primary vanadium species in the colloidal dispersion of nanoparticles of hydrated vanadium oxide. $V_2O_5 \cdot nH_2O$ films were then prepared by spreading 50 μL of $V_2O_5 \cdot nH_2O$ sol onto fluorine-doped tin oxide (FTO) glass substrates. After drying under ambient conditions for 24 h, the films were then annealed at 300 °C in four different annealing gas atmospheres: film 1, for 3 h in air; film 2, for 0.5 h in air, followed by 2.5 h in nitrogen; film 3, for 2.5 h in nitrogen, followed by 0.5 h in air; and film 4, for 3 h in nitrogen.

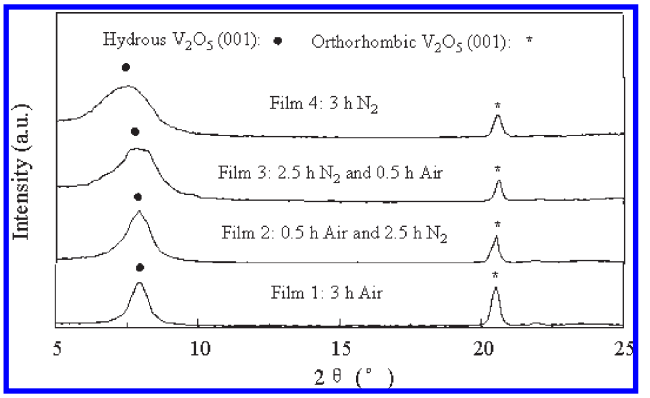

Figure 2. X-ray diffraction patterns of V_2O_5 xerogel films annealed in different air and nitrogen atmospheres at 300 °C after 3 h, showing the coexistence of both hydrous and orthorhombic vanadium oxide.

Scanning electron microscopy (SEM, Philips, JEOL JSM-7000), atomic force microscopy (AFM, Asylum Research MFP3D), and X-ray diffraction (XRD, Philips 1820 X-ray diffractometer) were carried out to characterize the morphology, surface roughness, and crystallization state of annealed films. X-ray absorption spectroscopy experiments were performed at the PNC-XOR bending magnet beamline (20-BM) of the Advanced Photon Source at Argonne National Laboratory. Measurements at the V K edge were performed in fluorescence mode. An electrochemical impedance spectroscopy study was carried out using a Salon 1260 impedance/gain-phase analyzer with a Pt foil as the counter electrode and 1 M $LiClO_4$ in propylene carbonate as the electrolyte. The frequency range was from 100 kHz to 0.05 Hz. Lithium-ion intercalation properties of V_2O_5 films were investigated using a standard three-electrode system, with 1 M $LiClO_4$ in propylene carbonate as the electrolyte, a Pt mesh as the counter electrode, and Ag/AgCl as the reference electrode. Chronopotentiometric (CP) tests were carried out in the voltage range from 0.6 to −1.4 V with a current density of 600 mA g^{-1}. The CP tests were performed using an electrochemical analyzer (CH Instruments, model 605B). The area of the working electrode used for all the electrochemical studies was 6.9 mm × 7.9 mm.

3. RESULTS AND DISCUSSION

The sol−gel-derived V_2O_5 films are homogeneous with a smooth and featureless surface morphology. No detectable cracks or pinholes are observed, and the film thickness is ∼1 μm. The porosity of the as-fabricated film at room temperature is estimated through density measurement and calculation to be about 54%. SEM images (not shown here) reveal no appreciable morphology difference between the as-fabricated V_2O_5 films and the films annealed in air and nitrogen. The surface roughness study was carried out by atomic force microscopy; the image of the film annealed in air for 3 h is shown in Figure 1. In a homogeneous region of 30 μm, the surface roughness is about 50 nm. No noticeable surface roughness difference is found on films annealed in different gas atmospheres. However, different annealing treatments do demonstrate appreciable influences on crystal structure and grain size. The X-ray diffraction (XRD) patterns of the four annealed films are compared in Figure 2.

dx.doi.org/10.1021/jp111847s |J. Phys. Chem. C 2011, 115, 4959–4965

Table 1. Interlayer Spacing and Grain Size of V_2O_5 Films Annealed in Different Atmospheres of Air and Nitrogen at 300 °C for 3 h

film	annealing gas	interlayer spacing (Å)	grain size (nm)
1	3 h air	11.0	14.3
2	0.5 h air +2.5 h N_2	11.1	11.6
3	2.5 h N_2 + 0.5 h air	11.2	6.4
4	3 h N_2	11.5	5.1

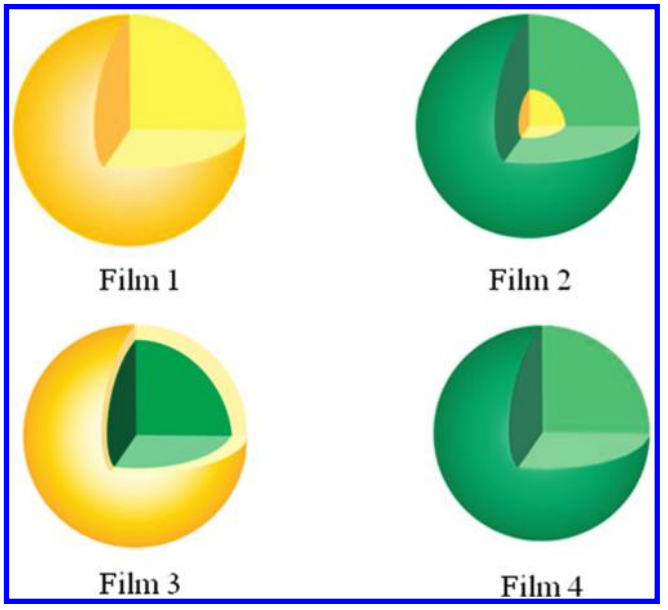

Figure 3. Schemes illustrating the different chemistry of V_2O_5 films 1−4 annealed in different air and nitrogen atmospheres with the yellow color representing the presence of the V^{5+} compound and the green color representing the presence of the V^{4+} compound.

Sol−gel-derived V_2O_5 film without thermal treatment exhibits only a hydrous phase, whereas after annealing at higher than 330 °C, it only exhibits an orthorhombic phase.[14] Films annealed at 300 °C in different gas atmospheres all exhibit both hydrous V_2O_5 and orthorhombic V_2O_5 phases, indicating that there is partial phase transition from hydrous V_2O_5 to orthorhombic V_2O_5. Film 1 (annealed only in air) is more crystallized than film 4 (annealed only in nitrogen); it possesses a more noticeable orthorhombic (001) peak, a smaller interlayer distance, and larger grain sizes (estimated by applying the Scherrer equation to the full width at half-maximum of the hydrous (001) peak[22,23]). Films 2 and 3 (annealed in both air and nitrogen atmospheres) have a crystallinity between the films annealed only in air or nitrogen. The interlayer distances and grain sizes of these films were calculated, and the results are summarized in Table 1. V_2O_5 films annealed in all conditions possess a similar interlayer distance of ∼11 Å, very close to the interlayer distance of hydrous V_2O_5 with 1.6 water molecules. However, there is a significant difference in grain size between the films annealed in nitrogen and air. The grain size of ∼5.1 nm in film 4 is about one-third of that in film 1 (14.3 nm). The grain sizes of films annealed in combined air and nitrogen treatments are between these two values. It should be noted that the crystallinity of film 2, treated, first, in air for 0.5 h and then in nitrogen for 2.5 h (grain size, 11.6 nm), is obviously better than that of film 3, treated in the reverse order (grain size, 6.4 nm), even though the annealing times under air and nitrogen are the same. This reveals that the initial annealing atmosphere is decisive for the final grain size, with air annealing contributing to grain growth far more than nitrogen annealing.

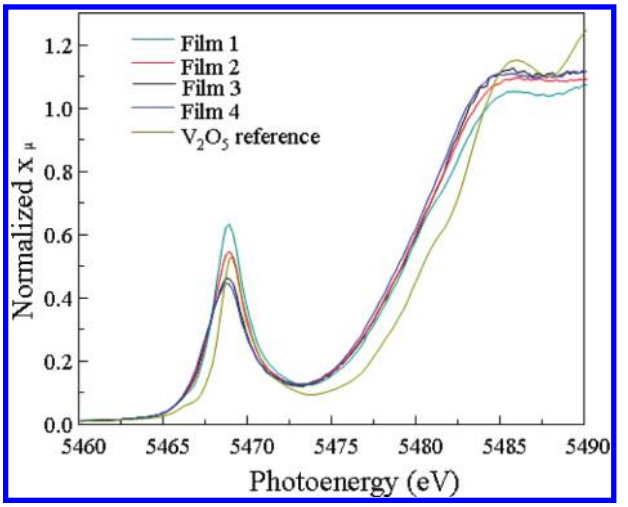

Figure 4. Normalized vanadium K-edge XANES of V_2O_5 xerogel films annealed in different air and nitrogen atmospheres at 300 °C for 3 h, showing edge an energy shift and pre-edge peak intensity change.

The four films possess not only different grain sizes but also a varied surface chemistry, as schematically illustrated in Figure 3. Nitrogen annealing induces the reduction of V^{5+} ions (represented as yellow) to V^{4+} ions (represented as green). As depicted, in film 1, there are no or few V^{4+} ions; in film 2, the film surface is covered by V^{4+} ions (green exterior); film 3 has a large amount of V^{4+} ions in the film interior (green), but the film surface V^{4+} is reoxidized to V^{5+} due to re-exposure to air; and film 4 has a V^{4+} ion interior as film 3, but no reoxidation of V^{4+} on the surface due to the application of only N_2 annealing.

The V ion oxidation states in the four films were studied by K-edge X-ray absorption spectroscopy (XAS). As the penetration length for X-rays with energy in the vicinity of the V K-edge is more than an order of magnitude larger than the effective thickness of the films (including porosity effects), this measurement is both bulk-sensitive and also insensitive to self-absorption effects. A comparison of the normalized V K-edge spectra is shown in Figure 4, together with the spectrum for a reference crystalline V_2O_5 sample. The relative absence of a structure beyond the absorption edge indicates that the sol−gel films have only a very short-range order. The directional dependence of the pre-edge, 1s → 3d transition (not shown) indicates a strong layering parallel to the substrate plane of the small, coherent V_2O_5 domains in the films. Examination of the spectra from sample 1 to sample 4 reveals that the edge energy is shifted to lower values when nitrogen annealing was used instead of air annealing, suggesting the presence of a lower average V oxidation state.[24] In addition to the shift in the edge energy, the intensity of the pre-edge peak also decreases, suggesting some combination of a more symmetric coordination of O atoms surrounding V atoms[25] and an increased occupation of V 3d-derived orbitals (i.e., again, a lower V oxidation state). The coexistence of a decreased pre-edge peak intensity and a chemical shift of the K edge to lower energy was also seen in the study of vanadium oxidation state degradation during repeated lithium-ion intercalation

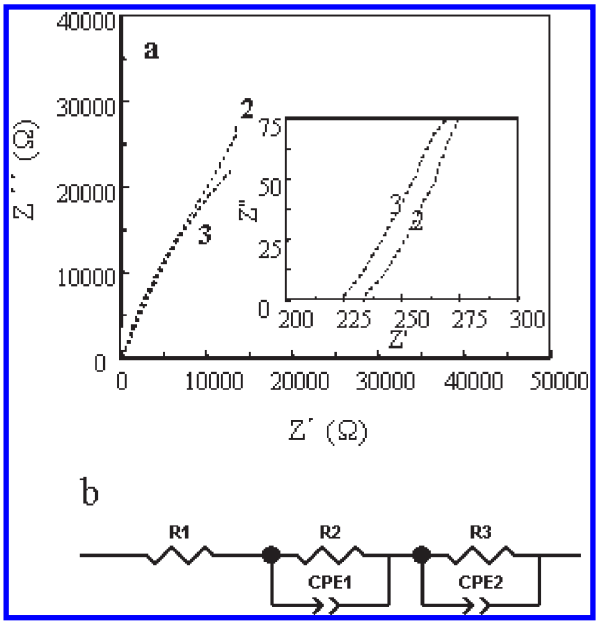

Figure 5. (a) ac impedance spectra presented as Nyquist plots of V_2O_5 films 2 and 3 annealed in reverse order of air and nitrogen atmospheres at 300 °C for 3 h and measured in 1 M $LiClO_4$ in propylene carbonate with testing frequencies from 100 kHz to 0.05 Hz (the inset shows the expanded plots at the high-frequency region). (b) The equivalent circuit used to fit the EIS data.

reported by Mansour et al.[26] For films 2 and 3 with combined air and nitrogen annealing, the edge energies are between those for film 1 annealed in air and film 4 annealed in nitrogen; film 3 has a noticeable decrease in the intensity of the pre-edge feature compared with film 2.

To further characterize the surface chemistry of films 2 and 3, an X-ray photoelectron spectroscopy study on films 2 and 3 was attempted. However, due to the sensitivity of the V^{4+} species to the ambient environment, the surface chemistry of the films was difficult to maintain after being taken out of tube furnace and the results failed to show the original surface chemistry of films 2 and 3.

The electrochemical impedance spectra (EIS) of films 2 and 3 are presented in Figure 5. Figure 5a shows the Nyquist plots of the measured films, and the inset depicts the expanded high-frequency region. Figure 5b shows the equivalent circuit that is used to fit the EIS data. In this circuit, R_1 represents the resistance of the electrolyte, R_2 is the resistance of the V_2O_5 film (or the electrode), and R_3 represents the charge-transfer resistance of the film/electrolyte interface, and the CPEs in the circuit are constant phase elements.[27,28] The parameters estimated through curve fitting are summarized in Table 2 together with those of film 1 and film 4, as reported in our earlier work.[15] The electrode resistance and charge-transfer resistance are found to change appreciably for films 2 and 3. Film 2 has a higher electrode resistance than film 3; however, the charge-transfer resistance is lower. Compared with film 4, film 2 has a similar charge-transfer resistance (82 vs 86 Ω), but the electrode resistance is noticeably higher (134 vs 114 kΩ), which could be due to a higher average V oxidation state, consistent with the XAS results. Charge-transfer resistance is critically important for lithium-ion intercalation capability due to the charge-transfer process at the electrode/electrolyte interface. Comparison of charge-transfer resistance

Table 2. Impedance Resistance Components for V_2O_5 Film Electrodes Annealed at 300 °C for 3 h in Different Atmospheres of Air and Nitrogen Determined by Fitting EIS Experimental Data Measured in 1 M $LiClO_4$ in Propylene Carbonate Using the Equivalent Circuit Shown in Figure 5b[a]

electrode	R_1 (Ω)[b]	R_2 (Ω)[b]	R_3 (Ω)[b]
film 1	244	166 150	125
film 2	232	133 730	82
film 3	224	120 620	97
film 4	237	113 540	86

[a] The data of films 1 and 4 are from ref 15. [b] R_1 = electrolyte resistance, R_2 = electrode resistance, R_3 = charge-transfer resistance.

shows the decreasing order of film 1 (125 Ω) > film 3 (97 Ω) > film 4 (86 Ω) ~ film 2 (82 Ω). Different annealing gas environments for these films are believed to be the cause that results in varied surface chemistry.[29] Compared to film 1, which is annealed only in air, film 4 is annealed only in nitrogen, which could reduce V^{5+} to more conductive V^{4+} species and decrease the surface charge-transfer resistance.[30] The surface chemistry mechanisms for film 2 and film 3 are a little more complicated. Film 3 is annealed, first, in nitrogen, but the surface is re-exposed to air for a short time, which could reoxidize V^{4+} species to V^{5+}, thus exhibiting a larger charge-transfer resistance than film 4. Film 2 is first annealed in air for a short time, followed by nitrogen treatment, which develops a similar surface chemistry and charge-transfer resistance as film 4.

The lithium-ion intercalation properties of films 2 and 3 were studied using chronopotentiometric (CP) tests. Figure 6 shows a comparison of the 1st and 30th CP curves measured at a charge/discharge current density of 600 mA g^{-1}. In Figure 6a, the initial CP curves of films 2 and 3 start the voltage drop from ~−0.07 and ~0.03 V, respectively. The charge and discharge curves of both films exhibit sloping manners as compared with the air-annealed film with a more well-defined plateau. The sloping curves suggest a less noticeable phase transition during the charge/discharge process and is characteristic of an intercalation host with less crystallinity due to the solid solution intercalation mechanism.[31] The discharge capacity and charge capacity of film 2 are 139 and 137 mA h g^{-1}, respectively, whereas those of film 3 are 129 and 133 mA h g^{-1}, respectively. It should be noted that the irreversible capacity of film 2 is only 2 mA h g^{-1}, and the Coulombic efficiency is as high as 98%, indicating good reversibility. In Figure 6b, showing the 30th cycle, whereas the discharge and charge capacities of film 2 increase to 147 and 148 mA h g^{-1}, those of film 3 decrease to 96 and 88 mA h g^{-1}. The irreversible capacity of film 2 is only 1 mA h g^{-1}, whereas that of film 3 is 8 mA h g^{-1}. After the comparison, it is clear that film 2 possesses good reversibility by maintaining a high Coulombic efficiency and charge/discharge capacity, whereas film 3 exhibits severe capacity degradation within 30 cycles.

Figure 7 shows a comparison of the long-term cyclic stability of all four films for lithium-ion intercalation measured with a current density of 600 mA g^{-1} over 50 continuous discharge/charge cycles. Film 2 has the best cyclic stability. Starting from the initial discharge capacity value of 139 mA h g^{-1}, the capacity increases slowly in the subsequent cycles before reaching a peak value of 156 mA h g^{-1} at the 15th cycle. The capacity decreases slowly in the following cycles but is still as high as 136 mA h g^{-1}, 98% of the initial value, after 50 cycles. The cyclic performance of

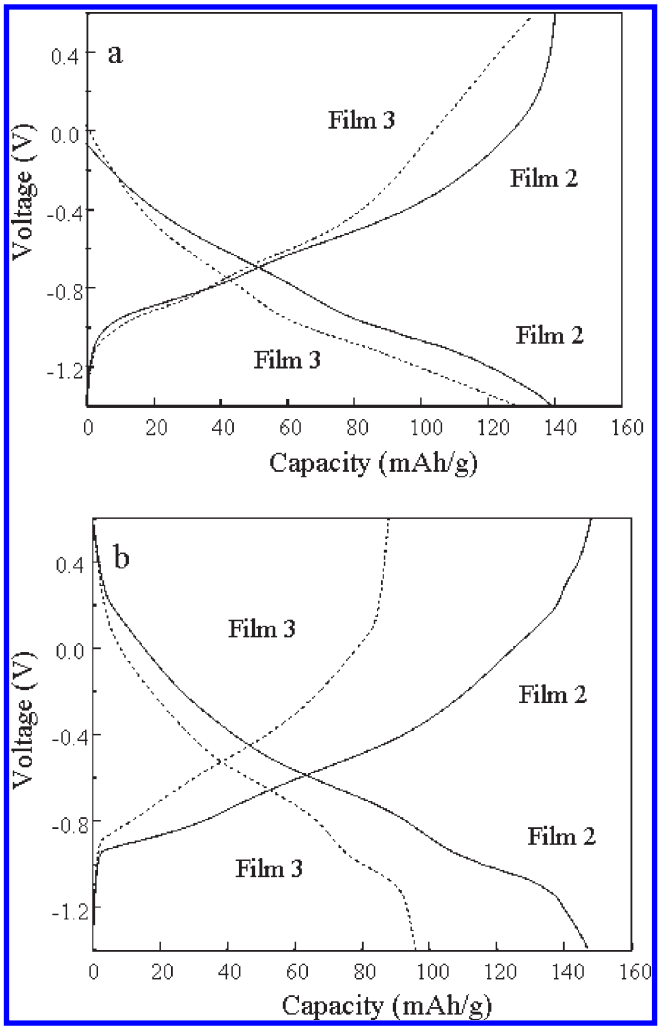

Figure 6. Chronopotentiometric discharge/charge curves in the (a) 1st and (b) 30th cycles at a current density of 600 mA g^{-1} of V_2O_5 films 2 and 3 annealed in a reverse order of air and nitrogen atmospheres at 300 °C for 3 h. The voltage window was 0.6 to −1.4 V vs Ag/AgCl as the reference electrode.

film 4 is very similar; it starts with a low discharge capacity of 68 mA h g^{-1} but is as high as 148 mA h g^{-1} after 50 cycles. Film 3 starts with a discharge capacity of 128 mA h g^{-1}, increasing to 136 mA h g^{-1} in the third cycle. The following cycles have a noticeable capacity degradation, and after 50 cycles, the capacity is only 75 mA h g^{-1}, 60% of the initial value. Film 1 has an even worse capacity degradation. In our earlier work,[15] we compared the cyclic stability of film 1 annealed only in air and film 4 annealed only in nitrogen and observed an obvious cyclic stability improvement of film 4 over film 1. The improved cyclic stability of the nitrogen-annealed film was attributed to the smaller grain size and the presence of surface defects, but we could not tell which was more important in improving cyclic stability. The comparison of the films annealed in combined air and nitrogen gases here reveals the obviously better cyclic stability of film 2, with a larger grain size and more surface defects, as compared with film 3, which has a smaller grain size and fewer surface defects. Both film 2 and film 4 possess surface defects and good cyclic stability, suggesting that the contribution of surface defects is the most important.

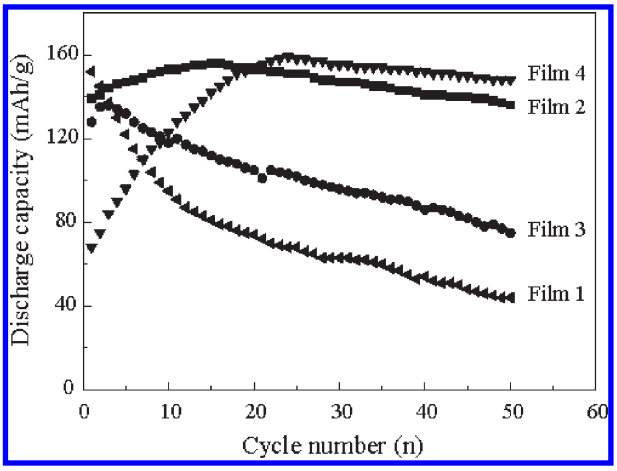

Figure 7. Li-ion intercalation discharge capacity of V_2O_5 films 1−4 annealed in different air and nitrogen atmospheres at 300 °C for 3 h as a function of cyclic numbers. The measurements were carried out in a potential window between 0.6 and −1.4 V vs Ag/AgCl as the reference electrode at a current density of 600 mA g^{-1}.

After the comparison of the physical and chemical properties of the four films and their lithium-ion intercalation properties, we clearly see that the intercalation cyclic stability is closely related to the defects present on the film surface. Film 2 (initially annealed in air, followed by nitrogen annealing) has an obviously larger grain size than film 4 (annealed only in nitrogen) and film 3 (annealed, first, in nitrogen, followed by air); however, the cyclic stability is comparable to that of film 4, which has a similar surface chemistry. It is also much better than film 3, which has more defects in the bulk, but fewer on the film surface. As revealed by the electrochemical impedance results, the presence of surface defects reduces the charge-transfer resistance and improves the charge-transfer kinetics while at the same time preventing active electrode material from dissolution in the electrolyte, which could improve cyclic stability. The importance of the electrode/electrolyte interface is well recognized for intercalation electrodes.[32,33] For all intercalation electrodes, especially nanostructured ones, there are two practical problems that need to be solved. First, the initial step of lithium-ion intercalation into the electrode involves the charge-transfer process of lithium ions from the electrolyte onto the surface of the electrode and the associated redox reactions involving the participation of electrons. If the extra charge cannot be readily transferred away after the reaction, charge accumulation would occur to impede more reactions.[34] To ensure complete redox reactions, good charge-transfer conductivity must be guaranteed. Second, during repeated intercalation/deintercalation cycles, the electrode surface could possibly dissolve into the electrolyte. This problem is more severe for nanostructured electrodes due to the large solid/liquid interfacial area.[35] The failure to maintain the surface morphology integrity directly lowers the intercalation capability, causing capacity degradation. Considering these two points, intercalation electrodes should possess good charge-transfer conductivity and surface integrity over long-term cycling to ensure favorable intercalation capacity and cyclic stability. To date, coating appears to be the most effective method to improve the surface charge-transfer process while, at the same time, preserving the morphology integrity of the active electrode.[36,37] Conductive carbon, metal, or oxides are often used, and improved cyclic stability has been reported.[38−40] However, the coating process is

dx.doi.org/10.1021/jp111847s |J. Phys. Chem. C 2011, 115, 4959–4965

often complicated and sometimes requires delicate equipment in order to achieve a homogeneous coating layer with good porosity. The basic requirement of electrolyte permeability after coating is always challenging to meet. Considering all of these practical problems, a layer of surface defects on the intercalation electrodes playing a similar role as an exterior coating might be a favorable alternative.

Besides enhancing charge-transfer conductivity and preserving the interface morphology integrity, surface defects also contribute to lithium-ion intercalation by shifting thermodynamics and improving kinetics. The presence of surface defects increases surface energy and could possibly serve as a nucleation center, thus facilitating phase transitions.[41] V_2O_5 nanorolls with surface cracks have exhibited a higher capacity than well-ordered nanoroll structures.[42] Additionally, TiO_2 nanotube arrays with surface defects were also found to possess a higher intercalation capacity than counterparts without surface defects.[43]

4. CONCLUSIONS

V_2O_5 films annealed at 300 °C under a combined annealing condition of air and nitrogen gas atmospheres exhibited varied crystallinity, vanadium oxidation states, and electrical conductivity. The film annealed in air for 0.5 h, then followed by N_2 for 2.5 h, was identified with better crystallinity and more composition defects on the surface as compared with films annealed in identical conditions but with a reversed air and nitrogen treatment order. In the lithium-ion intercalation test, this film also demonstrated a much improved lithium-ion intercalation capacity and cyclic stability. Starting from an initial value of 139 mA h g^{-1}, the discharge capacity increased to 156 mA h g^{-1} in the 15th cycle. After 50 cycles, the discharge capacity was still as high as 136 mA h g^{-1}, 98% of the initial value. The much improved lithium-ion intercalation capacity and cyclic stability are attributed to the presence of a surface defect layer that not only enhances the charge-transfer conductivity but also behaves like a protective coating layer to ensure the morphology stability of the V_2O_5 film and serves as a possible nucleation center to facilitate the phase transformation process during lithium-ion intercalation and deintercalation.

AUTHOR INFORMATION

Corresponding Author

*E-mail: gzcao@u.washington.edu.

ACKNOWLEDGMENT

This work was supported, in part, by the National Science Foundation (CMMI-1030048 and DMR-0605159), the Air Force Office of Scientific Research (AFOSR-MURI, FA9550-06-1-0326), the U.S. Department of Energy (DE-SC0002194), and Pohang University of Science and Technology, Korea. The operation of Sector 20 PNC-CAT/XOR is supported by the U.S. Department of Energy, Basic Energy Sciences, Office of Science (DE-FG03-97ER45629); the University of Washington; and grants from the Natural Sciences and Engineering Research Council of Canada. Use of the Advanced Photon Source was supported by the U.S. Department of Energy, Basic Energy Sciences, Office of Science (DE-AC02-06CH11357). D.W.L. would like to acknowledge the graduate fellowship (UIF) from the University of Washington Center for Nanotechnology (CNT). A.Q.P. would like to acknowledge the fellowship from the Chinese Scholarship Council. The authors also gratefully thank Dr. Mali Balasubramanian for the help with the X-ray absorption spectroscopy measurements and Shuhong Xie for the atomic force microscopy measurements.

REFERENCES

(1) Whittingham, M. S. *J. Electrochem. Soc.* **1976**, *123*, 315.
(2) Potiron, E.; Le Gal La Salle, A.; Verbaere, A.; Piffard, Y.; Guyomard, D. *Electrochim. Acta* **1999**, *45*, 197.
(3) Takahashi, K.; Wang, Y.; Cao, G. Z. *J. Phys. Chem. B* **2005**, *109*, 48.
(4) Wang, Y.; Cao, G. Z. *Chem. Mater.* **2006**, *18*, 2787.
(5) Chan, C. K.; Peng, H. L.; Twesten, R. D.; Jarausch, K.; Zhang, X. F.; Cui, Y. *Nano Lett.* **2007**, *7*, 490.
(6) Livage, J. *Chem. Mater.* **1991**, *3*, 579.
(7) Owens, B. B.; Passerini, S.; Smyrl, W. H. *Electrochim. Acta* **1999**, *45*, 215.
(8) Baddour, R.; Pereiraramos, J. P.; Messina, R.; Perichon, J. *J. Electroanal. Chem.* **1991**, *314*, 81.
(9) Chen, W.; Xu, Q.; Hu, Y. S.; Mai, L. Q.; Zhu, Q. Y. *J. Mater. Chem.* **2002**, *12*, 1926.
(10) Wang, Y.; Takahashi, K.; Shang, H. M.; Lee, K. H.; Cao, G. Z. *J. Phys. Chem. B* **2005**, *109*, 3085.
(11) Stojkovic, I.; Cvjeticanin, N.; Pasti, I.; Mitric, M.; Mentus, S. *Electrochem. Commun.* **2009**, *11*, 1512.
(12) Scarminio, J.; Talledo, A.; Andersson, A. A.; Passerini, S.; Decker, F. *Electrochim. Acta* **1993**, *38*, 1637.
(13) Wang, J. X.; Curtis, C. J.; Schulz, D. L.; Zhang, J. G. *J. Electrochem. Soc.* **2004**, *151*, A1.
(14) Wang, Y.; Shang, H. M.; Chou, T. P.; Cao, G. Z. *J. Phys. Chem. B* **2005**, *109*, 11361.
(15) Liu, D. W.; Liu, Y. Y.; Garcia, B. B.; Zhang, Q. F.; Pan, A. Q.; Jeong, Y. H.; Cao, G. Z. *J. Mater. Chem.* **2009**, *19*, 8789.
(16) Swider-Lyons, K. E.; Love, C. T.; Rolison, D. R. *Solid State Ionics* **2002**, *152*, 99.
(17) Ganduglia-Pirovano, M. V.; Sauer, J. *Phys. Rev. B* **2004**, *70*, 045422.
(18) Subramanian, V.; Zhu, H. W.; Wei, B. Q. *J. Phys. Chem. B* **2006**, *110*, 7178.
(19) Wu, Q. H.; Thissen, A.; Jaegermann, W.; Liu, M. *Appl. Surf. Sci.* **2004**, *236*, 473.
(20) Li, Z. Y.; Wu, Q. H. *J. Mater. Sci.* **2008**, *19*, S366.
(21) Fontenot, C. J.; Wiench, J. W.; Pruski, M.; Schrader, G. L. *J. Phys. Chem. B* **2000**, *104*, 11622.
(22) Cao, G. Z. *Nanostructures & Nanomaterials: Synthesis, Properties & Applications*; Imperial College Press: London, 2004.
(23) Birks, L. S.; Friedman, J. *J. Appl. Phys.* **1946**, *17*, 687.
(24) Giorgetti, M.; Passerini, S.; Smyrl, W. H.; Mukerjee, S.; Yang, X. Q.; Mcbreen, J. *J. Electrochem. Soc.* **1999**, *146*, 2387.
(25) Wong, J.; Lytle, F. W.; Messmer, R. B.; Maylotte, D. H. *Phys. Rev. B* **1984**, *30*, 5596.
(26) Mansour, A. N.; Smith, P. H.; Balasubramanian, M.; McBreen, J. *J. Electrochem. Soc.* **2005**, *152*, A1312.
(27) Xiao, P.; Liu, D. W.; Garcia, B. B.; Sepehri, S.; Zhang, Y. H.; Cao, G. Z. *Sens. Actuators, B* **2008**, *134*, 367.
(28) Xiao, P.; Garcia, B. B.; Guo, Q.; Liu, D. W.; Cao, G. Z. *Electrochem. Commun.* **2007**, *9*, 2441.
(29) Ganduglia-Pirovano, M. V.; Hofmann, A.; Sauer, J. *Surf. Sci. Rep.* **2007**, *62*, 219.
(30) Eder, D.; Kramer, R. *J. Phys. Chem. B* **2004**, *108*, 14823.
(31) Wang, Y.; Takahashi, K.; Lee, K.; Cao, G. Z. *Adv. Funct. Mater.* **2006**, *16*, 1133.
(32) Pyun, S. I.; Bae, J. S. *J. Power Sources* **1997**, *68*, 669.
(33) Fu, L. J.; Liu, H.; Li, C.; Wu, Y. P.; Rahm, E.; Holze, R.; Wu, H. Q. *Solid State Ionics* **2006**, *8*, 113.
(34) Olson, C. L.; Ballard, I. *J. Phys. Chem. B* **2006**, *110*, 18286.

(35) Aurbach, D.; Markovsky, B.; Salitra, G.; Markevich, E.; Talyossef, Y.; Koltypin, M.; Nazar, L.; Ellis, B.; Kovacheva, D. *J. Power Sources* **2007**, *165*, 491.
(36) Kim, Y. J.; Kim, H.; Kim, B.; Ahn, D.; Lee, J. G.; Kim, T. J.; Son, D.; Cho, J.; Kim, Y. W.; Park, B. *Chem. Mater.* **2003**, *15*, 1505.
(37) Li, C.; Zhang, H. P.; Fu, L. J.; Wu, Y. P.; Ram, E.; Holze, R.; Wu, H. Q. *Electrochim. Acta* **2006**, *51*, 3872.
(38) Odani, A.; Pol, V. G.; Pol, S. V.; Koltypin, M.; Gedanken, A.; Aurbach, D. *Adv. Mater.* **2006**, *18*, 1431.
(39) He, B. L.; Dong, B.; Li, H. L. *Electrochem. Commun.* **2007**, *9*, 425.
(40) Hu, Y. S.; Guo, Y. G.; Dominko, R.; Gaberscek, M.; Jamnik, J.; Maier, J. *Adv. Mater.* **2007**, *19*, 1963.
(41) Liu, D. W.; Cao, G. Z. *Energy Environ. Sci.* **2010**, *3*, 1218.
(42) Sun, D.; Kwon, C. W.; Baure, G.; Richman, E.; MacLean, J.; Dunn, B.; Tolbert, S. H. *Adv. Funct. Mater.* **2004**, *14*, 1197.
(43) Liu, D. W.; Zhang, Y. H.; Xiao, P.; Garcia, B. B.; Zhang, Q. F.; Zhou, X. Y.; Jeong, Y. H.; Cao, G. Z. *Electrochim. Acta* **2009**, *54*, 6816.